Eur Biophys J (2009) 38:649–661
DOI 10.1007/s00249-009-0422-4

ORIGINAL PAPER

# Convolution-based one and two component FRAP analysis: theory and application

**Astrid Tannert · Sebastian Tannert · Steffen Burgold · Michael Schaefer**

Received: 9 October 2008 / Revised: 22 January 2009 / Accepted: 29 January 2009 / Published online: 24 February 2009


**Abstract** The method of fluorescence redistribution after photobleaching (FRAP) is increasingly receiving interest in biological applications as it is nowadays used not only to determine mobility parameters per se, but to investigate dynamic changes in the concentration or distribution of diffusing molecules. Here, we develop a new simple convolution-based approach to analyze FRAP data using the whole image information. This method does not require information about the timing and localization of the bleaching event but uses the first image acquired directly after photobleaching to calculate the intensity distributions, instead. Changes in pools of molecules with different velocities, which are monitored by applying repetitive FRAP experiments within a single cell, can be analyzed by means of a global model by assuming two global diffusion coefficients with changing portions. We validate the approach by simulation and show that translocation of the YFP-fused PH-domain of phospholipase C$\delta$1 can be quantitatively monitored by FRAP analysis in a time-resolved manner. The new FRAP data analysis procedure may be applied to investigate signal transduction pathways using biosensors that change their mobility. An altered mobility in response to the activation of signaling cascades may result either from an altered size of the biosensor, e.g. due to multimerization processes or from translocation of the sensor to an environment with different viscosity.

**Keywords** Fluorescence recovery after photobleaching · Mobility-based biosensors · Diffusion · Multiple diffusion coefficients · Global data analysis

**Abbreviations**

| | |
|---|---|
| AOI | Area of interest |
| AOTF | Acousto-optic tunable filter |
| CCD | Charge-coupled device |
| CLSM | Confocal laser scanning microscopy |
| FRAP | Fluorescence redistribution after photobleaching |
| HBS | HEPES-buffered solution |
| HEK | Human embryonic kidney |
| PH | Pleckstrin homology |
| $PI(4,5)P_2$ | Phosphatidylinositol-4,5-bisphosphate |
| PLC$\delta$1(PH) | PH domain of phospholipase C$\delta$1 |
| RSS | Residual sum of squares |
| TIR | Total internal reflection |
| YFP | Yellow fluorescent protein |

**Electronic supplementary material** The online version of this article (doi:10.1007/s00249-009-0422-4) contains supplementary material, which is available to authorized users.

A. Tannert · M. Schaefer (✉)
Rudolf-Boehm-Institut für Pharmakologie und Toxikologie, Universität Leipzig, Härtelstraße 16-18, 04107 Leipzig, Germany
e-mail: michael.schaefer@medizin.uni-leipzig.de

S. Tannert
PicoQuant GmbH, Berlin, Germany

S. Burgold
Department of Molecular Pharmacology and Cell Biology, Neurowissenschaftliches Forschungszentrum, Charité, Universitätsmedizin Berlin, Berlin, Germany

*Present Address:*
S. Burgold
Institut für Neuropathologie, Zentrum für Neuropathologie und Prionforschung (ZNP), Ludwig-Maximilians-Universität München, Munich, Germany

## Introduction

The classical method for determining diffusion coefficients of pools of fluorescent molecules in living cells is fluorescence redistribution after photobleaching (FRAP), which was first described by Axelrod (1976) and has since been widely employed to investigate diffusion. In a biological context such photobleaching experiments are mainly performed to define the biophysical properties of cellular compartments (Lippincott-Schwartz et al. 2003) and to get insight into protein localization, transport and interaction (Reits and Neefjes 2001; Lippincott-Schwartz et al. 2003; Klonis et al. 2002) as well as into the organization of lipids and membrane-associated proteins (Klonis et al. 2002). Algorithms to extract binding kinetics of proteins out of FRAP measurements are currently being developed (Dushek et al. 2008; Sprague and McNally 2005). In pharmaceutical research, the mobility and delivery of drug molecules can be tested by FRAP, too (De Smedt et al. 2005; Meyvis et al. 1999).

Moreover, since the diffusion of biological probes depends on the viscosity of their microenvironment, translocation of these probes often results in an altered mobility. Most prominently, the diffusion coefficients of membrane-associated and cytosolic proteins differ by more than one order of magnitude (Teruel and Meyer 2000; Reits and Neefjes 2001; Klonis et al. 2002). Therefore, protein translocation events between the cytoplasm and the plasma membrane, which are frequently found during the activation of signaling cascades, can be analyzed by repetitively monitoring the mobility of fluorescence-tagged proteins (Tannert et al. 2008). Translocation of proteins involved in signal transduction is rarely complete and often involves only minor fractions of the total available marker proteins. Therefore, it is frequently not possible to detect these translocations by classical imaging approaches like CLSM. To unravel even minute changes in the amount of plasma membrane-associated and cytosolic proteins, we have recently developed a setup to monitor cells expressing fluorescent proteins with prismless evanescent wave illumination and selectively point-bleach parts of the image (Tannert et al. 2008). Since the penetration depth of the evanescent field is restricted to 100–200 nm, total internal reflection (TIR) fluorescence microscopy is the method of choice to selectively excite molecules at the plasma membrane and in the cytoplasm near the plasma membrane. Thus, by combining TIR fluorescence imaging with FRAP analysis, the sensitivity of the detection of weak plasma membrane association or dissociation processes can be significantly increased.

Most approaches to calculate the mobility of biomolecules from FRAP experiments extract information from the redistribution curve of fluorescence only in the bleached spot. A number of mathematical models has been developed to extract the diffusion coefficient from such measurements (for review see Chen et al. 2006). Nowadays, spatial information is readily available in most fluorescence microscopy setups, e.g. using digital videoimaging or confocal laser scanning microscopy (CLSM). Furthermore, computing power has increased dramatically, making it possible to analyze whole image series in reasonable time. When spatial information is analyzed by a fully analytical model, it is necessary to have exact knowledge of the location of the bleached region, its form, the occurrence of the bleaching event, and the geometry of the investigated sample (Kubitschek et al. 1994; Wedekind et al. 1996; Seiffert and Oppermann 2005; Sbalzarini et al. 2005). This information is difficult to obtain for the following reasons: (1) the diameter of small bleached spots is affected by the point spread function (PSF) of the laser beam, (2) photobleaching may be incomplete and (3) out-of-focus bleaching in the light cone of the laser beam may result in a complex shape of the bleached volume. Furthermore, diffusion takes place already during the bleaching period, making it difficult to determine the exact starting point of fluorescence redistribution, especially when diffusion is fast or the photobleaching kinetics is slow, even though models to take this process into account have been developed (Braga et al. 2004). These drawbacks are partly overcome using spatial fourier analysis (Tsay and Jacobson 1991; Berk et al. 1993) and Hankel transform analysis (Jonsson et al. 2008). Here we develop another, simple analysis method of spatial FRAP experiments by convolving the first postbleach image with the solution of the diffusion equation for a pixel source. Inhomogeneities in the label distribution are compensated for by dividing each postbleach image by a mean of prebleach images. This pixel convolution method does not necessarily require spatial and temporal knowledge of the bleach event and it does not require complete photobleaching in the bleached spot. By simulation of FRAP experiments (as would occur using our combined TIR/FRAP setup) assuming diffusion of molecules within the cytoplasm and plasma membrane we validate our data analysis model and determine its restrictions. We then show that this approach provides a sensitive technique to detect the activation of a signaling pathway in vivo by applying repetitive FRAP measurements and analyzing the diffusion of a YFP-fused biosensor for phosphatidylinositol lipids, YFP-PLC$\delta$1(PH), with a global two component model.

## Materials and methods

### Cell culture and transfection

HEK293 cells (ATCC, Manassas, VA) were maintained in minimal essential medium with Earle's salts supplemented

with 10% fetal calf serum, 100 µg/ml streptomycin and 100 U/ml penicillin at 37° and 5% $CO_2$. Cells were seeded onto poly-L-lysine-coated glass coverslips in 35-mm cell culture dishes. Transfections with expression plasmids encoding the rat histamine H1 receptor and YFP-PLC$\delta$1(PH) (Sinnecker and Schaefer 2004) were performed using Fugene 6 transfection reagent (Roche Molecular Biochemicals, Mannheim, Germany) according to the manufacturer's instructions at a confluency of about 70%.

### Confocal fluorescence imaging

All experiments were performed 18–48 h after transfection in HEPES-buffered solution (HBS), containing 10 mM HEPES (pH 7.4), 134 mM NaCl, 6 mM KCl, 1 mM $MgCl_2$, 1 mM $CaCl_2$, 5.5 mM glucose and 0.2% (w/v) bovine serum albumin. Glass coverslips were mounted onto the stage of an inverted CLSM (LSM 510Meta, Carl Zeiss MicroImaging GmbH, Jena, Germany). Imaging of the YFP fusion proteins was carried out using the 488-nm line of an $Ar^+$ laser with a dichroic mirror (reflective below 488 nm), a 505 nm long pass emission filter and an $\alpha$-Plan Fluar 100×/1.45 objective (Zeiss).

### Combined spot photobleaching and TIR fluorescence measurements

A setup for combining measurements under TIR illumination with spot photobleaching was described previously (Tannert et al. 2008) and was used with slight modifications. Briefly, YFP was excited using the 488-nm line of an $Ar^+$-laser (Lasos, Germany) for spot photobleaching and the 514-nm line with reduced power for TIR fluorescence imaging. The beampaths used for TIR excitation and spot photobleaching were separated and recombined using two dichroic mirrors reflective below 505 nm (Chroma, Rockingham, VT). For switching between the laser lines and power reduction of the 514-nm line used for TIR fluorescence imaging an acousto-optic tunable filter (AOTF, A-A Opto-Electronic, Orsay Cedex, France) was used. For photobleaching with the 488-nm line, collimated light was focused by the objective into a diffraction-limited spot, which had a diameter of 250–300 nm similar to the calculated size of the PSF (see below and Fig. 1). Image acquisition was performed with a cooled CCD camera (Sensicam QE, PCO, Kelheim, Germany) using TillVision software (TILL Photonics, Gräfelfing, Germany).

### Simulation of synthetic data and data analysis

The parameters chosen to simulate synthetic FRAP data are described in the Results section. Pixel intensities and timings of the TIR fluorescence measurements were extracted from a 16-bit TIFF-data file and a time code data file, respectively, generated by the acquisition software. The pixel size was calculated from the magnification of the objective and the pixel size of the chip of the CCD-camera. In 2× binning mode, typically used for our experiments, the pixel size in the image was 129 nm. The data processing and fitting algorithms are described in detail in the Results section. Algorithms were programmed in C using the GNU scientific library (Galassi et al.).

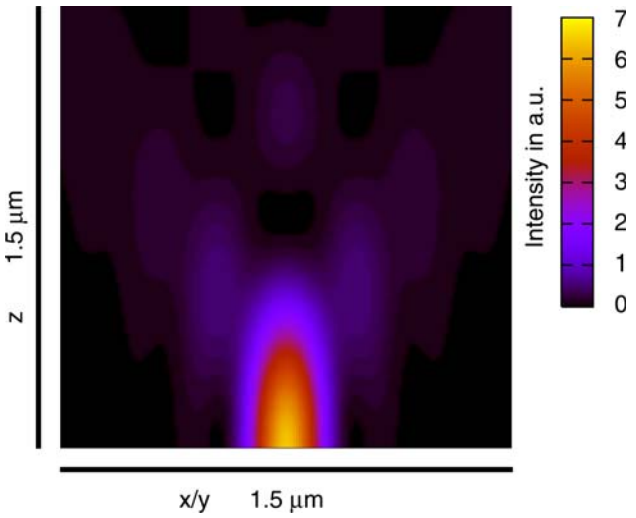


**Fig. 1** Calculated PSF for bleaching with a 488 nm laser beam using a 100× objective with NA = 1.45. Intensity is given in a.u. The dimensions of the image are 1.5 × 1.5 µm. The focal plane is located at the bottom of the image

## Theory

### Model for FRAP data analysis

Diffusion of molecules is described by Fick's second law, which reduces to two dimensions for membrane-associated substances:

$$\frac{\partial C}{\partial t} = D\left(\frac{\partial^2 C}{\partial \tilde{x}^2} + \frac{\partial^2 C}{\partial \tilde{y}^2}\right), \quad (1)$$

with $C$ representing the concentration of molecules and $D$ the diffusion coefficient. Please note that we denote continuous coordinates as $\tilde{x}$ and $\tilde{y}$, here.

During video-FRAP measurements, fluorescence is sampled into images consisting of discrete square pixels. The recorded fluorescence intensity of one pixel $I_{pix}$ is proportional to the number of fluorophores within the pixel area. The number of fluorophores in one pixel is given by integrating the concentration over the area, therefore:

$$I_{\mathrm{pix}}(x,y,t) \propto \int_{x-h}^{x+h}\int_{y-h}^{y+h} C(\tilde{x},\tilde{y},t)\mathrm{d}\tilde{x}\mathrm{d}\tilde{y} \tag{2}$$

with $h = 0.5$ if coordinates $x$ and $y$ are measured in discrete pixel units.

The initial distribution of the marker molecules at $t = 0$ is accessible from the image acquired after photobleaching. It is assumed that this initial concentration can be approximated as homogenous within one pixel. Therefore, Eq. 1 has to be solved for the case that molecules are initially confined in a finite region (one square pixel at $-0.5 \le x \le 0.5$; $-0.5 \le y \le 0.5$) with a concentration $C_0$ and diffuse towards infinity. The concentration at time $t$ at the coordinates $\tilde{x}, \tilde{y}$ is given by

$$C(D,\tilde{x},\tilde{y},t) = \frac{1}{4}C_0\left(\mathrm{erf}\frac{h-\tilde{x}}{2\sqrt{Dt}} + \mathrm{erf}\frac{h+\tilde{x}}{2\sqrt{Dt}}\right) \times \left(\mathrm{erf}\frac{h-\tilde{y}}{2\sqrt{Dt}} + \mathrm{erf}\frac{h+\tilde{y}}{2\sqrt{Dt}}\right) \tag{3}$$

under these constraints (Crank 1975). The error function erf is defined as

$$\mathrm{erf}(z) = \frac{2}{\sqrt{\pi}}\int_0^z \exp(-u^2)\mathrm{d}u \tag{4}$$

Since diffusion processes originating from one initial region (pixel) can be assumed independent of that from any neighboring one, the fluorescence intensity at any time is given by the convolution of the initial intensity map $I(i, j, 0) \propto C_0(i, j)$ with the diffusion distribution function followed by an integration over the pixel areas. The linearity of the convolution allows for exchanging the order of integration and convolution.

$$I(D,x,y,t) = \sum_i\sum_j I(i,j,0) \times \int_{x-i-h}^{x-i+h}\int_{y-j-h}^{y-j+h} C(D,\tilde{x},\tilde{y},t)\mathrm{d}\tilde{x}\mathrm{d}\tilde{y} \tag{5}$$

Having $k$ populations of molecules exhibiting different diffusion coefficients $D_k$ with portions $a_k$, the intensity distribution of any measured postbleach image is given as a superposition of the intensity distributions that originate from each single homogenously diffusing species. Assuming an additional immobile fraction with the portion $a_{\mathrm{IM}}$, the total image fluorescence intensity is modeled as:

$$I_{\mathrm{tot}}(x,y,t) = a_{\mathrm{IM}}I(x,y,0) + \sum_k a_k(I(D_k,x,y,t)) \tag{6}$$

Numerical evaluation showed that if $Dt$ is higher than a critical value of 5 pixel$^2$, the solution of Eq. 1 for an infinite small point source diffusing towards infinity becomes a good approximation for the intensity distribution originating from each pixel, giving:

$$I_{\mathrm{pix}}(x,y,t) \propto \frac{M}{4\pi Dt}\exp\frac{-(x^2+y^2)}{4Dt} \tag{7}$$

where $M$ represents the amount of diffusing molecules which were located at time $t = 0$ at the point $x = y = 0$, i.e. in the pixel for which the diffusional process is calculated. Therefore, when $Dt$ was higher than this critical value, the intensity of each pixel was assumed as an infinite small point and Eq. 7 was used to calculate the convolution:

$$I_{\mathrm{tot}}(x,y,t) = a_{\mathrm{IM}}I(x,y,0) + \sum_k a_k \times \left(\sum_i\sum_j I(i,j,0)\frac{1}{4\pi D_k t}\exp\frac{-(x-i)^2-(y-j)^2}{4D_k t}\right) \tag{8}$$

This simplified model reduced the computational burden as it is not necessary to evaluate the more complex function erf and the subsequent integration over the pixel area when the value of $Dt$ exceeds 5 pixel$^2$.

## Results

### Simulation of FRAP and development of a procedure for data analysis

For analysis of FRAP data from spot photobleaching measurements in TIR fluorescence configuration, we regard the first postbleach image as initial condition (Sniekers and van Donkelaar 2005). The following recorded postbleach images (denoted simply as postbleach images here) are used to fit the mobility parameters. To this end, the intensity profile of the first postbleach image is convolved with the solution of the diffusion equation in two dimensions to model the intensity development over time for given diffusion coefficients. By minimizing the residual sum of squares (RSS) between the modeled intensity development and the measured postbleach images, the mobility parameters are determined. This allows for the extraction of diffusion coefficients without exact knowledge of the bleach geometry and timing.

When all fluorescent molecules are assumed to diffuse with the same velocity, this is referred to as one component model. Analysis of images where two distinct mobilities contribute to the intensity distribution was performed by superposing two diffusional processes each with a specific diffusion coefficient and portion. This is referred to as two component model (Gordon et al. 1995).

*Generation of synthetic data*

The described procedure of FRAP data analysis requires a two-dimensional diffusion process of the investigated molecules. For plasma membrane-bound proteins this is clearly the case, though diffusion of cytosolic proteins occurs in three dimensions. However, the data may be regarded as pseudo-two-dimensional, since bleaching occurs along the PSF of laser illumination, whose distribution in axial direction is much broader than in the radial plane (Meyvis et al. 1999; Sprague et al. 2004). In our experimental setup, the depth of the bleaching beam is about 400 nm in the *z*-direction, whereas the TIR illumination has a penetration depth of about 130 nm.

To test if this assumption is justified and to revise the goodness of data analysis, we simulated synthetic FRAP data to model typical biological experiments. A diffusion process with two separate diffusion coefficients $D_1 = 0.2$ μm$^2$/s, typical for membrane-bound molecules, and $D_2 = 5$–$10$ μm$^2$/s, similar to values found for cytosolic proteins, was assumed. Two-dimensional diffusion was chosen for the slow component, while that of the fast species was assumed to occur in three dimensions. The portions of the slow and fast fractions were varied, while their sum was normalized to unity, in order to make these amplitude coefficients directly represent interconvertible fractions.

The bleaching profile was simulated by calculating the three-dimensional PSF for a 100× objective with NA = 1.45 and 488 nm excitation wavelength (Fig. 1) according to a previously described formula (Jonkman and Stelzer 2002). The maximal bleaching efficiency in the focal plane was assumed as 95%. The bleaching profile was stored in a set of matrices representing *z*-stacks in a distance of 10 nm, where the first matrix was set to the focal plane. This matrix corresponds to the plasma membrane in TIR fluorescence configuration. Matrices were calculated up to an axial distance from the focal plane of 4 μm, where the bleaching intensity per matrix element had dropped to less than 1% of that within the focal plane. Each matrix was composed of 519 × 519 elements which were assumed to have a size of 10 nm × 10 nm. The evolution of this initial distribution was calculated for 20 time steps with an interval of 25 ms by convolution with the respective diffusion kernels for diffusion in two or three dimensions. While slow diffusion was simulated as a two-dimensional process in the focal plane matrix only, the fast diffusion process was calculated three-dimensionally with reflection at the focal plane (which would correspond to the cellular plasma membrane). Image data were then simulated by calculating the mean of the first 13 matrices proximal to the focal plane, which represent the TIR-volume and binning 13 × 13 matrix elements in *xy*-direction to get synthetic images with a pixel size of 130 nm, similar to our measured data. Since typical data obtained from biological samples, i.e. from cells transiently expressing an autofluorescent fusion protein measured in TIR fluorescence configuration, are afflicted by noise with an SD of about 2%, experimental noise was emulated by adding random numbers of a Gaussian distribution with a mean of zero and a SD ranging from 0.1 to 5% to simulated images.

*Analysis of synthetic FRAP data*

In a first approach, we fitted synthetic data to a model assuming only one diffusion coefficient (one component model). Minimization of the RSS between the synthetic FRAP data and model data from convolution of the first synthetic FRAP matrix with the solution of the diffusion equation was achieved by Brent's algorithm (Brent 1973). When only the fast species was present (i.e. diffusion was simulated completely three-dimensionally), its diffusion coefficient was slightly overestimated (i.e. by 10–20%) probably due to the assumption of pseudo-two-dimensionality. As expected, an intermediate diffusion coefficient was calculated, when the data set comprised both velocities, and the RSS was highest when the fractions of both velocities were about equal, i.e., when the assumption of one uniform diffusion coefficient was least accurate (Fig. 2a). The fitted apparent diffusion coefficient obtained by the one component model was only slightly influenced by the addition of noise.

Results were then compared with evaluations using a two component model. The application of the two component model was justified for all data sets that contained two velocities and for fractions of one of the components as low as 5% in the 95% confidence interval, tested by an *F*-test of the decrease in the RSS (Gordon et al. 1995). When 1% or more noise was added, the determination of diffusion coefficients was inaccurate and failed totally in some cases (i.e. when one component was present only in low amounts) using the two component model and a single photobleaching cycle (Fig. 2b).

To increase the robustness of data fits, we therefore applied global data analysis over multiple (>20) FRAP cycles for two component data, assuming two species diffusing with distinct diffusion coefficients not altered in a series of data sets, but with changing portions. This would apply to repetitive FRAP measurements at an identical region within a single cell, where the amount of membrane-bound and cytosolic molecules changes over time. Both diffusion coefficients of a series of FRAP data sets were linked and fitted by Brent's algorithm while the corresponding portions of each diffusing species were calculated by means of generalized linear least square regression using QR-decomposition for each FRAP data

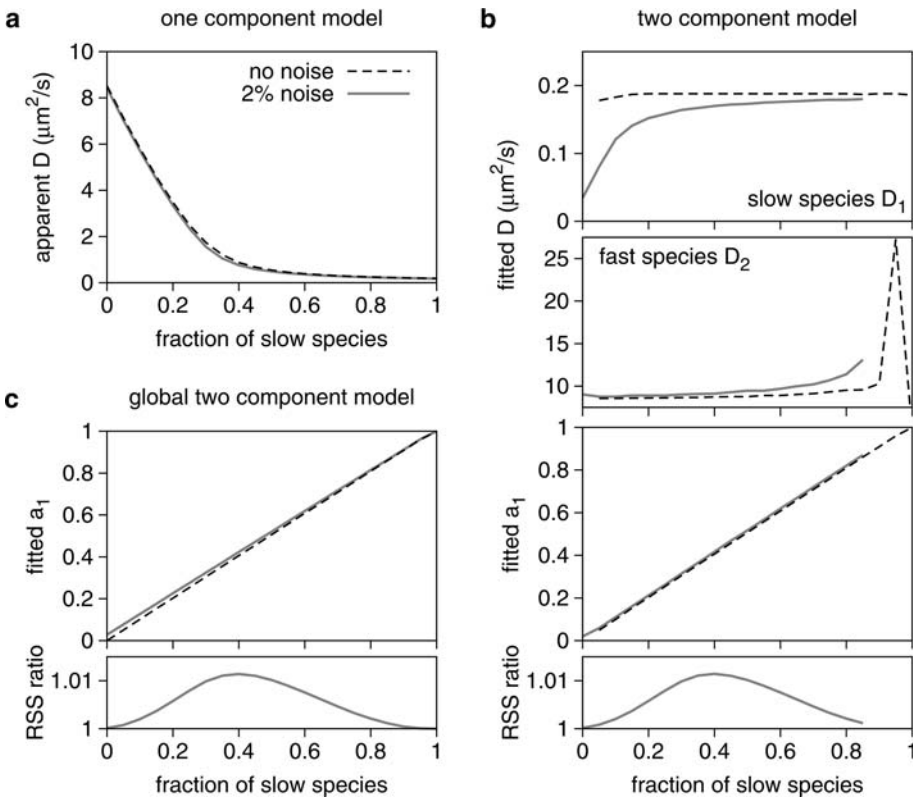


**Fig. 2** Fit of synthetic data with one or two diffusion coefficients. Diffusion in an area of 5.2 μm × 5.2 μm with a central circular bleached region according to a bleaching PSF was simulated with $D_1 = 0.2$ μm²/s and $D_2 = 7.5$ μm²/s and fractions $a_1$ of the slow diffusion coefficient ranging from 0 to 1. The diffusion process occurring with the slower diffusion coefficient $D_1$ was calculated two-dimensionally while the faster one was simulated to occur in a three-dimensional space. Random numbers with a mean of zero and a SD of 0.02 were added to simulate noise as it occurs in a biological experiment (*solid lines*). For comparison, data without added noise were fitted (*dashed lines*). In a first approach, simulated data were fitted using a one component model (**a**). The diffusion coefficients determined with a two component model and the determined fraction a1 of the slow diffusion coefficient are shown in (**b**). The ratio of the RSS obtained from fitting data with 2% noise to the one component model versus the two component model is highest when the fractions of both diffusion coefficients are about equal. Fractions $a_1$ of the slow diffusion coefficient determined by a a global data fit and the ratio of the RSS of the one component model versus the global two component model for data with 2% noise are shown in (**c**)

set. The whole fitting algorithm was adapted from the variable projection approach (Golub and Pereyra 1973, 2003). Using the global approach, diffusion coefficients and their portions were more reliably determined without outliers. Determination of the portions of fast and slow diffusing species was still possible with sufficient accuracy when up to 5% noise was added (see Fig. 2c showing the determined portions of the slow diffusing species of data containing 2% noise). Hence, the global model was applied to all further evaluations. For given diffusion coefficients $D_1 = 0.2$ μm²/s and $D_2 = 7.5$ μm²/s, the determined values were $D_1 = 0.18$ μm²/s, $D_2 = 9.4$ μm²/s for data with 2% noise or $D_1 = 0.19$ μm²/s, $D_2 = 8.6$ μm²/s for data without noise. As already expected from the one component data analysis, the fast diffusion coefficient was slightly overestimated (by 10–20%). This effect became more pronounced by the addition of noise (overestimation by 20–30%), while the slow diffusion coefficient was slightly underestimated when noise was added. Since the residuals were strongly influenced by noise, we tested for the justification of the two component model by comparing the RSS of the two component analysis to that obtained by the one component analysis. The ratio of the RSS from one versus two component fits should be higher than unity to justify the application of the two component model. This is demonstrated by the analysis of our simulated data set, where this ratio is highest in cases where equal amounts of fast and slow species are present. Since the RSS is strongly influenced by the noise, this difference becomes more pronounced for higher signal-to-noise ratios.

Using the intensity profile of the first postbleach image as initial condition does not affect the accuracy of the determination in cases where only one diffusing species is present. In cases of more than one diffusing species, an equilibrium distribution of diffusing molecules is assumed by the model, i.e. in the initial postbleach image, the amounts of fast and slow diffusing species should be the same in each pixel. However, since diffusion occurs

already during the process of photobleaching, the distributions of fluorescent markers with different mobility will differ with time, i. e., rapidly diffusing molecules will reach the bleached region earlier than slow ones. To estimate the error by using the intensity profile of an image acquired immediately after photobleaching, we simulated data assuming two diffusing species with $D_1 = 0.2$ μm$^2$/s and $D_2 = 5$–$10$ μm$^2$/s and changing fractions. These data were globally fitted to the two component model with initial distributions that would occur at simulation time points 2–20 ms after photobleaching. While preciseness of the evaluation of $D_1$ was hardly altered under these conditions, the value of the fast diffusion coefficient was further overestimated. Deviations in the determination of the portions of fast and slow diffusing species were highest in cases where both fractions are present to a similar amount. Under these conditions, the fraction of the slowly diffusing species was overestimated (Fig. 3). Since this inaccuracy is most efficiently prevented by decreasing the delay of the first postbleach image acquisition, we conclude that the first postbleach image should be acquired immediately after photobleaching, ideally not later than 5 ms after initiating photobleaching. Alternatively, by increasing the size of the imaged area (i.e. by binning pixels) the overestimation of the slowly diffusing species may also be reduced when fast image acquisition after bleaching is not possible. The estimated maximal deviations in the portions of slow and fast diffusing molecules are summarized in Supplementary Table 1 for various experimental conditions. We note that when designing an experimental setup to determine more than one diffusing component using FRAP and the first postbleach image as initial condition,

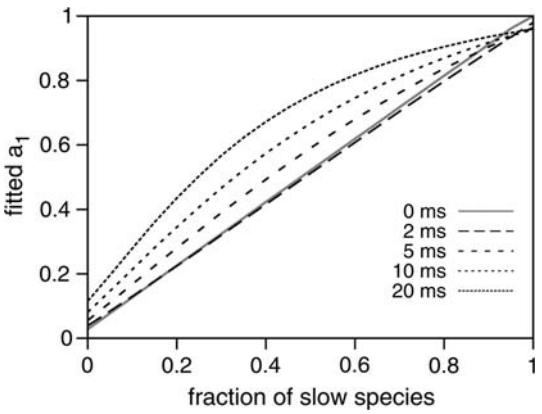


**Fig. 3** Influence of using a postbleach image instead of the exact bleach image as initial condition. A diffusion process was simulated with the same parameters as described in Fig. 2 and 2% noise was added. Data were fitted globally using either the exact bleach image (*solid line*) or a postbleach image as it would occur at the indicated time after the bleaching, as initial condition. The fitted fraction $a_1$ of the slow diffusion coefficient is plotted versus the fraction of this diffusion process that was simulated

one should be careful to decrease the time between bleaching and image acquisition to a minimum and to check theoretically if this required time interval is short enough to ensure that data analysis is feasible with sufficient accuracy.

*Processing of data from biological experiments*

Knowing the experimental conditions that should be chosen for optimal two component analysis from the modeling, we have investigated the redistribution of the fluorescent protein YFP-PLC$\delta$1(PH), which indicates receptor-induced PI(4,5)$P_2$ hydrolysis by changing from a plasma membrane-bound state to a freely diffusible, soluble state. The redistribution of YFP-PLC$\delta$1(PH) is well known from confocal imaging, so we chose this biosensor to prove the reliability of our method. Mobility-based characterization of membrane association is, however, even more advantageous for biosensors with lower translocation efficiencies that are not easily detectable using CLSM (Tannert et al. 2008).

A typical TIR fluorescence image of a cell expressing YFP-PLC$\delta$1(PH), which is typically membrane-associated under resting conditions, is shown in Fig. 4a. A region within the cell was selected and monitored continuously before and after point bleaching in the center of this region for 2–5 ms (Fig. 4b). To account for inhomogeneities of the marker distribution (as shown in Fig. 4d), 16 images preceding the bleach event were recorded. Postbleach images were divided by the mean of prebleach images to obtain normalized intensities (see Fig. 4c, e) (Lu et al. 2008). Since averaged prebleach images still contain a significant amount of noise, multiplication of this noise into all postbleach images may feign an immobile fraction. This problem was easily obviated by dividing the first postbleach image (which served as initial condition for modeling diffusion) by the mean of eight prebleach images and all following postbleach images by eight different averaged prebleach images. To account for continuous bleaching during prebleach image acquisition, the first postbleach image was re-normalized by dividing this image by the mean intensity of its outer pixels. The recorded and normalized bleach image was surrounded by pixels with an intensity of unity to calculate the convolution. Intensity fluctuations due to bleaching within the following measured postbleach images would significantly impair the data analysis since they would introduce a offset between experimental and modeled data (Supplementary Fig. 1a). We simulated experimental data with a loss of fluorescence intensity between the postbleach images as it would occur due to exponential bleaching. As shown in Supplementary Fig. 1b, the portion of the slow diffusing species is severely underestimated when 0.1% of bleaching is introduced

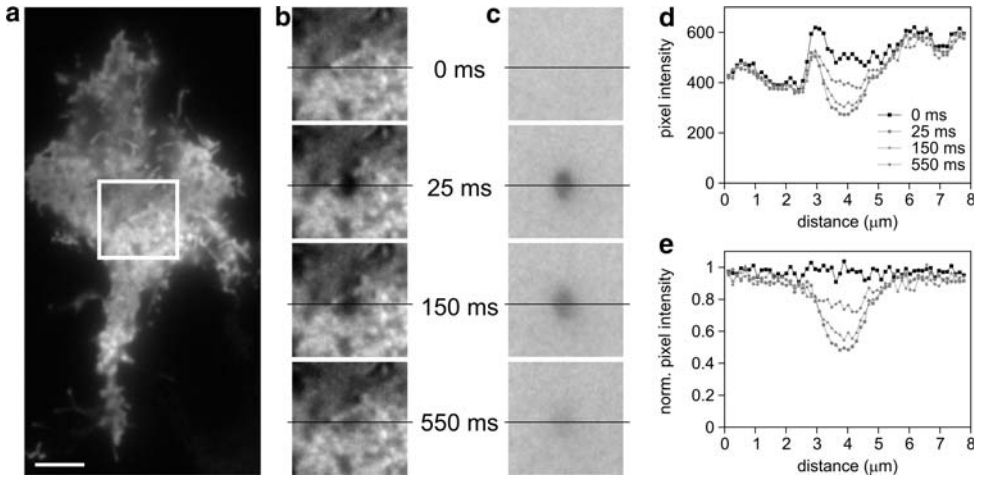


**Fig. 4** A typical FRAP experiment with TIR illumination. **a** Cells expressing a YFP-tagged PLC$\delta$1(PH), which binds to PI(4,5)$P_2$, were investigated using TIR fluorescence. For the subsequent FRAP analysis, an AOI was selected (*box*), which is fully located within the confines of the cell. **b** The area drawn in (**a**) was continuously monitored at low laser power of the 514-nm line in TIR fluorescence configuration. After acquisition of a series of prebleach images, a spot in the center of the image was bleached by applying a point-focused 488-nm laser for 3 ms. The distribution of fluorescence after bleaching was monitored by acquisition of 20 postbleach images every 25 ms in TIR fluorescence configuration (514 nm) at low laser power. **c** Uneven distribution of fluorescence intensity is eliminated by dividing the postbleach frames by the mean of the recorded prebleach images. **d** and **e** Fluorescence profiles along the lines indicated in (**b**) and (**c**), respectively, for the selected images

between each postbleach image. Under different modeled conditions (introduction of noise and a postbleach acquisition delay times) the fast diffusion coefficient was overestimated to unacceptable values (>1,000 $\mu m^2/s$), making a global two-component analysis unreasonable. For this reason we determined the mean intensity of each measured postbleach image and calculated the mean intensity of the model image at the corresponding time point of fluorescence recovery (using a preceding QR decomposition for the model images of this time point) at the given set of diffusion coefficients to determine the amount of photobleaching. The intensities of the model images at each time point were than scaled by the bleaching factor followed by a QR-decomposition to determine the fractions of fast and slow species for the whole recovery series. With this correction procedure, we are able to reliably fit experimental data, even when 0.1% bleaching is introduced between each of the postbleach images (see Supplementary Fig. 1b).

Translocation of YFP-PLC$\delta$1(PH) from the plasma membrane to the cytosol was induced by stimulating the cells coexpressing the histamine H1 receptor with 100 μM histamine, leading to a PLC-mediated PI(4,5)$P_2$ hydrolysis (Fig. 5a). The translocation of YFP-PLC$\delta$1(PH) was rapid and transient, several minutes after stimulation with histamine parts of the biosensor re-located to the plasma membrane. Changes in the mobility of the marker protein were monitored by continuous repetitive FRAP cycles in TIR fluorescence configuration for 13 min (Fig. 5b). After 10 FRAP cycles in resting cells, translocation was stimulated by addition of 100 μM histamine. Optimal diffusion coefficients for the one component and for the global two component model were determined by minimizing the RSS.

The receptor-induced PI(4,5)$P_2$-hydrolysis resulted in an increase in the apparent diffusion coefficient as quantified applying the one component model (Fig. 5c). Since it is reasonable to assume that the measured fluorescence redistribution profile is the result of two diffusion processes with a fast cytoplasmic and a slower plasma membrane-attached population of YFP-PLC$\delta$(PH), we fitted data globally to obtain the two diffusion coefficients of soluble and membrane-bound YFP-PLC$\delta$(PH) and their fractions (Fig. 5d). The diffusion coefficients determined from the individual cell shown in Fig. 5b for the cytosolic and membrane-associated fraction were 8.5 and 0.11 $\mu m^2/s$ with 67% confidence intervals ranging from 7.8 to 9.2 and 0.10 to 0.13 $\mu m^2/s$, respectively. We tested for an immobile fraction by assuming an additional component with an unchanged fluorescence distribution (i.e., that of the normalized first postbleach image) over time, whose fractions were determined by QR-decomposition (see above). In our experimental data the determined portion of this fraction was negligible. Therefore, an immobile fraction was not considered for the proteins used here. The surface of the RSS for one component analysis as well as for the global determination of both diffusion coefficients exhibits a single and global minimum (see Fig. 6). Since there are no local minima, the determination of the diffusion coefficients is unique and robust. The fraction of the slow plasma

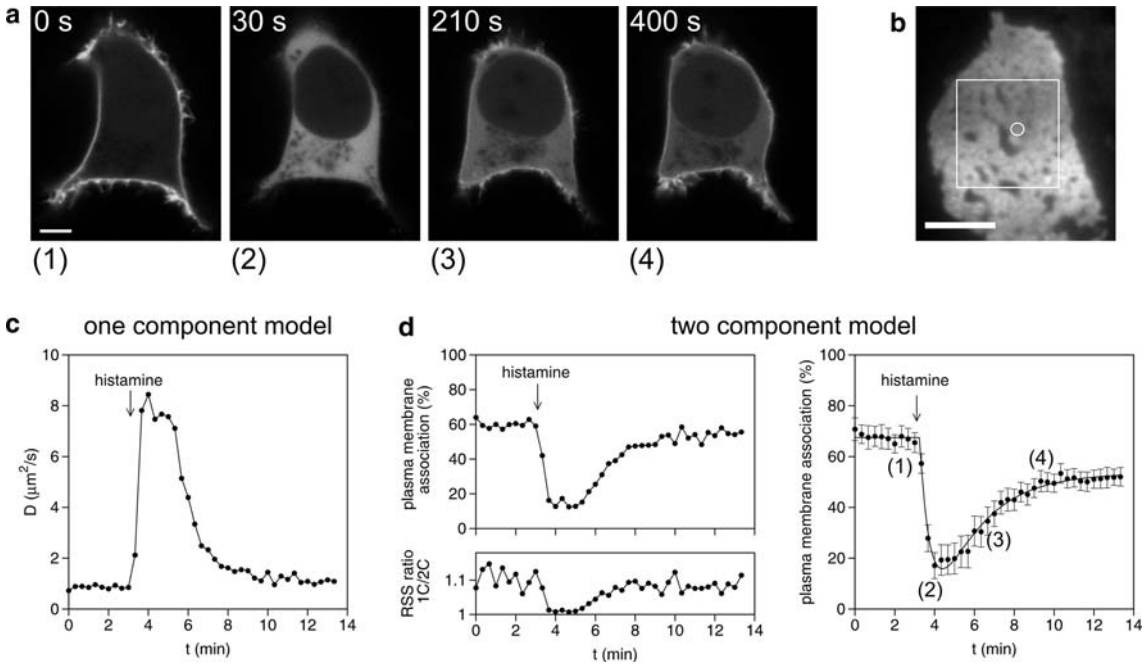


**Fig. 5** Histamine-induced redistribution of YFP-PLC$\delta$1(PH) from the the plasma membrane to the cytosol. **a** Fluorescence of HEK293 cells expressing YFP-PLC$\delta$1(PH) and the histamine H1 receptor was monitored continuously using a CLSM while cells were stimulated with 100 μM histamine. A representative example of YFP-PLC$\delta$(PH) translocation is shown. *Bar* 5 μm. **b** A cell expressing YFP-PLC$\delta$(PH) was selected in TIR fluorescence configuration for continuous FRAP experiments. *Bar* 5 μm. **c** Diffusion coefficients of repetitive FRAP experiments using the cell shown in (**b**). The area of the *box* shown in **b** was included into analysis. Bleaching was performed at the indicated spot in **b**. After 10 bleach experiments, cells were stimulated by addition of 100 μM histamine resulting in PI(4,5)$P_2$ hydrolysis and an increase in the apparent diffusion coefficient calculated by the one component model due to loss of plasma membrane association. **d** Applying the global two component model on the same data set, diffusion coefficients of 8.4 and 0.11 μm$^2$/s were determined for the cytosolic and membrane-bound fractions, respectively. The percentage of the slow fraction representing membrane-bound molecules is shown in the left panel for the time course of the experiment. The ratio of the RSS obtained from the one component and two component model is highest when about equal fractions of molecules reside in the cytosol and in the plasma membrane. *Right panel* membrane association during histamine stimulation are depicted as mean ± SE of seven independent measurements

membrane-associated species was about 60% before stimulation and transiently decreased to 10% after stimulation (Fig. 5d). The relatively low portion of plasma membrane-associated YFP-PLC$\delta$1(PH) in resting cells is unexpected when compared with confocal images of unstimulated cells showing that the biosensor is almost completely membrane-bound (Fig. 5a). This discrepancy is indicative of fast local binding and rebinding events rather than a firm binding to PI(4,5)$P_2$ (see "Discussion"). The absolute width of the 67% confidence interval for the determination of the portions of diffusing species was always lower than 2.5%. The increased ratio of the RSS obtained from one- versus two-component model analysis at conditions where a part of the fluorophores is cytosolic and membrane-associated, respectively, is similar to that found in our simulations with 1% noise and assuming about equal portions of two diffusing species. Several repetitive FRAP experiments were performed in independent cells showing a high reproducibility (Fig. 5d) of the time course and percentage of the transient redistribution upon histamine stimulation. The resulting diffusion coefficients were 7.1 ± 0.9 μm$^2$/s and 0.21 ± 0.05 μm$^2$/s ($n = 7$ experiments) for the cytosolic and the membrane bound fractions, respectively. The kinetics of the initial translocation process was rapid with a half-time of about 23 s, which was close to the temporal resolution of our FRAP approach. Redistribution of the biosensor to the plasma membrane, and thus inactivation of the signal, followed rapidly after activation with a half-time of about 1.5 min. Remarkably, only about 85% of the initial translocated biosensor were re-directed to the plasma membrane indicating that the signaling cascade was not totally inactivated, at least during the 10-min time course of our measurements.

## Discussion

The application of FRAP measurements has recently been extended to investigations of dynamic processes such as the translocation of proteins from and to the plasma membrane in living cells applying repetitive bleaching in a single cell (Tannert et al. 2008). In this application, two

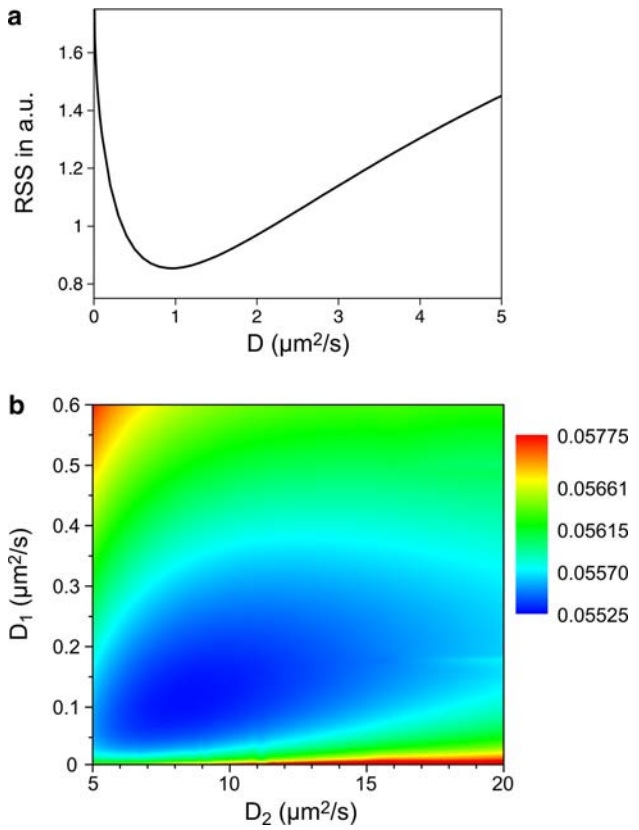


**Fig. 6** Determination of minimal RSS using the one component and the two component model. **a** Normalized postbleach images of HEK293 cells expressing YFP-PLC$\delta_1$(PH) from Fig. 5 were fitted to the one component model by minimizing RSS, yielding an apparent diffusion coefficient of 0.97 $\mu m^2/s$. The distribution of the RSS over diffusion coefficients is shown. **b** RSS-surface of diffusion coefficients of the same cell during histamine-stimulation using the global two component model. The global two component FRAP analysis shown in Fig. 5d resulted in the plotted RSS-surface

species of molecules diffusing with different velocities are monitored, and changes in their respective quantities are used to investigate, e.g. the activation of signaling cascades. This technique is especially useful when the portion of translocating biosensors is low compared to the total amount of expressed biosensor proteins. This study aimed at developing a suitable and simple algorithm to analyze especially two component FRAP data from repetitive measurements using the whole image information.

Therefore, a convolution-based method has been developed and validated. By analyzing various sets of synthetic FRAP data, we validated the analysis approach and identified conditions that should be chosen for biological experiments. We have shown that three-dimensional diffusion may be regarded as pseudo-two-dimensional in special cases with some limitations. This simplification is only valid when three-dimensional diffusion in the cytoplasm is not restricted by any boundaries, e.g. by sequestration of fluorescent particles in organelles (Sbalzarini et al. 2005). In our case we have shown that two-dimensional data analysis provides acceptable results even for high numerical aperture objectives as needed for prismless TIR fluorescence imaging, which do not fulfill the requirement of bleaching a cylindrical shape (Braeckmans et al. 2003). Since signal-to-noise ratios at typical experimental conditions (about 1–3% noise) significantly impair the determination of diffusion coefficients and their portions using the two component model, global fitting has been applied to all repetitive FRAP experiments, which yielded appropriate results using synthetic or experimental data.

We are aware that the assumption of Brownian movement of molecules within the plasma membrane is a simplification (Kusumi et al. 2005), since the plasma membrane is not a homogenous medium. Moreover, the influence of a possible membrane curvature of the plasma membrane leading to an underestimation of the membrane-associated diffusion coefficient and an anisotropic diffusion process (Sbalzarini et al. 2006) is neglected in our model. One should further emphasize that the method does not apply for photobleaching fluorescence redistribution analysis in more complex shaped structures like organelles, for which models for specific three-dimensional diffusion analysis have been developed (Ölveczky and Verkman 1998; Sbalzarini et al. 2005). However, our simplified diffusion model is useful to discriminate molecules with different velocities in or near the plasma membrane of cells by means of their mobility.

A variety of other FRAP data analysis methods that use the whole image information has been developed mostly to address specific problems like inhomogenous diffusion (Siggia et al. 2000; Sniekers and van Donkelaar 2005). In these approaches, magnification is quite low so that whole cells (or even tissues) are monitored and a relative large area is bleached in the FRAP experiment. To determine the apparent diffusion coefficients in the ER, Siggia et al. (2000) projected the recorded image to a mesh of about $10 \times 10$ pixels and calculated the apparent diffusion coefficient for each element independently. Only a single diffusion coefficient was determined for each point, which is sufficient since all molecules are assumed to diffuse with the same velocity in this model. By contrast, Sniekers and van Donkelaar (2005) attempted to discriminate the diffusional processes within cells and extracellular matrix in the proliferation zone of the growth plate. The exact location of the different areas has to be defined by imaging beforehand in this approach, however. Recently, image-based FRAP analysis has been applied to determine the diffusion of a FRET-based biosensor for Src activity (Lu et al. 2008). Information obtained by FRAP experiments was used to correct for diffusional displacement of the biosensor and, thus, to determine the exact subcellular localization of Src activity. Since all biosensors are

assumed to diffuse with the same velocity, the authors did not consider different diffusion coefficients and used rather large bleach areas with bleaching times of 15 s and recorded recovery points every 1–10 s.

In contrast to these approaches, using our experimental setup a relative small area is monitored with high magnification and using a diffraction-limited spot for photobleaching. This ensures that image acquisition and bleaching is fast to monitor dynamic processes by repetitive FRAP events. Since only a small spot is bleached in our approach, total fluorescence redistribution is rapidly equilibrating enabling fast repetitive FRAP experiments (up to six FRAP cycles per minute for membrane-bound proteins or up to two FRAP cycle per second for soluble proteins). As indicated above, the first postbleach image has to be obtained only a few milliseconds after bleaching is initiated under these experimental conditions ensuring that fast and slow diffusing molecules are equally distributed at the beginning of the redistribution process which allows for an accurate two component data analysis. Fast image acquisition and short bleaching times are, thus, essential to obtain appropriate results using our fitting procedure with different diffusing species.

In fact, most previous two component analysis methods used the recovery profile of the bleached spot only (Gordon et al. 1995). With the nowadays available increased computational power we are able to use the intensity profile of the whole recorded image for a convolution-based data analysis. Since this method increases the number of data points used for the analysis, the fitting results become more precise especially at lower signal-to-noise ratios. In addition, the number of free fitting parameters is reduced (as we do not need to fit the shape of the bleach spot in our model). Recently, a method using Hankel transforms has been introduced to increase preciseness of two component analysis (Jonsson et al. 2008). This is another image-based method for FRAP data analysis, where circular averaged images are used. However, even though this method increases the signal-to-noise ratio and, thus, improves the determination of the two diffusion coefficients, it is still necessary to precisely locate the bleaching region. Moreover, this analysis method requires nearly circular image and bleach geometry. In contrast, our model of FRAP data analysis is completely independent of image geometry and bleach shape. Furthermore, due to global data analysis over multiple FRAP experiments at the same cellular location, we achieve a high degree of fitting robustness.

For data analysis from images with inhomogenous fluorescence distribution, we have applied a compensation method by dividing the images acquired after spot-photobleaching by the mean of prebleach images yielding appropriate normalization of the postbleach images similar to a previously described normalization procedure (Lu et al. 2008). Another method to compensate for fluorescence inhomogeneities introduced by van Donkelaar and coworkers (Sniekers and van Donkelaar 2005) uses a subtraction of postbleach from prebleach images rather than a division. The subtraction would be justified when inhomogeneities arise from areas with high and low concentrations of marker molecules, further assuming that the number of diffusing molecules is constant in the whole imaged area. In our measurements using TIR illumination, inhomogeneities in the marker distribution mostly originate from a different distance between coverslip and plasma membrane. In this case, a ratioing between post- and prebleach images is more suitable to account for inhomogenous fluorescence distribution, since in areas that appear brighter, also molecules diffusing in and out of these areas would appear with higher intensity than in darker areas. Moreover, inhomogenous fluorescence distribution may also be caused by organelles which cannot be populated by fluorescence markers, in which case the ratioing is justified, too. Very bright spots are under-weighted in the data analysis, which can be advantageous since such spots often represent aggregates or encapsulated molecules which do not participate in the diffusion process. We note that using the division method, signal-to-noise ratios may be decreased in darker areas. This can be compensated for by weighting the RSS of such areas lower. Thereby, areas with no significant fluorescence intensities in the prebleach images would completely exclude from the analysis thus increasing the robustness in the presence of cell boundaries or large unpopulated organelles. We conclude that ratiometric normalization is highly suitable for the TIR/FRAP data analysis and gives appropriate results as demonstrated experimentally.

The global two component FRAP analysis method was successfully applied to analyze the transient translocation of the YFP-tagged PLC$\delta$1(PH) biosensor protein from the plasma membrane to the cytosol upon PI(4,5)$P_2$ hydrolysis. The diffusion coefficient of PLC$\delta$1(PH) was reported markedly higher in a previous study (Brough and Irvine 2005), compared to our results for this protein in its plasma membrane-associated form. This discrepancy is likely to result from the analysis approach, since in the previous study no cytosolic fraction was assumed. Indeed, we have found similarly high diffusion coefficients for YFP-PLC$\delta$1(PH) in unstimulated cells when applying a one-component analysis. We conclude that even PLC$\delta$1(PH) molecules that appear to be firmly plasma membrane-associated as inferred by their fluorescence distribution, still undergo local unbinding and rebinding events at the subsecond timescale, leading to the detection of an "effective diffusion" which is in fact a cytosolic diffusion that is only short-lived (Sprague et al. 2004). The global two component data analysis seems to describe the

diffusional processes at the plasma membrane more reliably, detecting fast diffusing molecules that were previously not discriminated from slow, plasma membrane-bound ones. However, the precise evaluation of the underlying process of such phenomena was beyond the scope of this study.

Membrane association of proteins has previously been analyzed using a FRAP approach with variable bleaching beam size (Henis et al. 2006; Shvartsman et al. 2007). This method allows to discriminate between fluorescence recovery caused by diffusion in the membrane and by fast cytosolic exchange. This is a very elegant approach to analyze the amount of membrane associated proteins if the exchange with the cytoplasm is faster than the diffusion within the membrane. Since the receptor-induced translocation of biosensors is relatively slow compared to the fluorescence redistribution after spot photobleaching, this method is not applicable for our purpose to describe translocation of biosensors in signaling events. It might, however, be used to analyze the postulated fast unbinding and rebinding events of YFP-PLC$\delta$1(PH) in resting cells (see above) in future studies.

The variation of the diffusion coefficients of YFP-PLC$\delta$1(PH) within different cells found in our experiments most likely reflects different apparent viscosities in these cells. By contrast, the variation of repeatedly determined diffusion coefficients in a single cell is low (SD of individual determinations typically amounts to less than 10%). Since the difference between cytosolic and membrane-confined mobilities exceeds one order of magnitude and since velocities of bound and unbound fractions are robustly quantified by the global fitting procedure, the variability in the determination of membrane-associated and cytosolic fractions was even lower (absolute values of SD of individual determinations are typically in the range of 5%). This enables a very precise determination of membrane-associated and cytosolic fractions.

Since binding to the plasma membrane is associated with pronounced changes in the lateral mobility, we could show that a two component FRAP model and convolution-based global data analysis sensitively detect binding or unbinding of proteins to membranes, which is ideally monitored in the TIR fluorescence configuration. However, the data analysis method can be equally well applied to confocal bleaching experiments when the bottom layer of a cell or, with some modifications, when a section through a cell including a plasma membrane are monitored with sufficient time resolution and fast photobleaching. State-of-the-art AOTF-controlled confocal microscopical devices easily fulfill these requirements. Likewise, repetitive FRAP measurements in combination with our data analysis algorithm may also be applicable to spinning disk confocal microscopes and to epifluorescence microscopes if equipped with an appropriate focused laser to perform the spot photobleaching.

## References


Axelrod D, Koppel DE, Schlessinger J, Elson E, Webb WW (1976) Mobility measurement by analysis of fluorescence recovery after photobleaching. Biophys J 16:1055–1069

Berk DA, Yuan F, Leuning M, Jain RK (1993) Fluorescence photobleaching with spatial fourier analysis: measurement of diffusion in light-scattering media. Biophys J 65:2428–2436

Braeckmans K, Peeters L, Sanders NN, De Smedt SC, Demeester J (2003) Three-dimensional fluorescence recovery after photobleaching with the confocal scanning laser microscope. Biophys J 85:2240–2252

Braga J, Desterro JM, Carmo-Fonseca M (2004) Intracellular macromolecular mobility measured by fluorescence recovery after photobleaching with confocal laser scanning microscopes. Mol Biol Cell 15:4749–4760

Brent RP (1973) Algorithms for minimization without derivatives (Prentice-Hall series in automatic computation). Prentice-Hall, Englewood Cliffs

Brough D, Bhatti F, Irvine RF (2005) Mobility of proteins associated with the plasma membrane by interaction with inositol lipids. J Cell Sci 118:3019–3025

Chen Y, Lagerholm BC, Yang B, Jacobson K (2006) Methods to measure the lateral diffusion of membrane lipids and proteins. Methods 39:147–153

Crank J (1975) The mathematics of diffusion, 2nd edn. Oxford University Press, Oxford

De Smedt S, Remaut K, Lucas B, Braeckmans K, Sanders N, Demeester J (2005) Studying biophysical barriers to DNA delivery by advanced light microscopy. Adv Drug Deliv Rev 57:191–210

Dushek O, Das R, Coombs D (2008) Analysis of membrane-localized binding kinetics with FRAP. Eur Biophys J 37:627–638

Galassi M, Davies J, Theiler J, Gough B, Jungman G, Booth M, Rossi F (2006) Gnu scientific library reference manual, 2nd edn

Golub GH, Pereyra V (1973) The differentiation of pseudo-inverses and nonlinear least squares problems whose variables separate SIAM. J Numer Anal 10:413–432

Golub GH, Pereyra V (2003) Separable nonlinear least squares: the variable projection method and its applications. Inverse Problems 19:R1–R26

Gordon GW, Chazotte B, Wang XF, Herman B (1995) Analysis of simulated and experimental fluorescence recovery after photobleaching. Data for two diffusing components. Biophys J 68:766–778

Henis YI, Rotblat B, Kloog Y (2006) FRAP beam-size analysis to measure palmitoylation-dependent membrane association dynamics and microdomain partitioning of Ras proteins. Methods 40:183–190

Jonkman JEN, Stelzer EHK (2002) Resolution and contrast in confocal and two-photon microscopy. In: Diaspro A (ed) Confocal and two-photon microscopy Willey-Liss, New York, pp 101–125

Jonsson P, Jonsson MP, Tegenfeldt JO, Hook F (2008) A method improving the accuracy of fluorescence recovery after photobleaching analysis. Biophys J :biophysj.108.134874

Klonis N, Rug M, Harper I, Wickham M, Cowman A, Tilley L (2002) Fluorescence photobleaching analysis for the study of cellular dynamics. Eur Biophys J 31:36–51

Kubitschek U, Wedekind P, Peters R (1994) Lateral diffusion measurement at high spatial resolution by scanning microphotolysis in a confocal microscope. Biophys J 67:948–956

Kusumi A, Nakada C, Ritchie K, Murase K, Suzuki K, Murakoshi H, Kasai RS, Kondo J, Fujiwara T (2005) Paradigm shift of the plasma membrane concept from the two-dimensional continuum fluid to the partitioned fluid: High-speed single-molecule tracking of membrane molecules. Annu Rev Biophys Biomol Struct 34:351–378

Lippincott-Schwartz J, Altan-Bonnet N, Patterson GH (2003) Photobleaching and photoactivation: following protein dynamics in living cells. Nat Cell Biol 5:S7–S14

Lu S, Ouyang M, Seong J, Zhang J, Chien S, Wang Y (2008) The spatiotemporal pattern of Src activation at lipid rafts revealed by diffusion-corrected FRET imaging PLoS. Comput Biol 4:e1000127

Meyvis TKL, De Smedt SC, Van Oostveldt P, Demeester J (1999) Fluorescence recovery after photobleaching: a versatile tool for mobility and interaction measurements in pharmaceutical research. Pharm Res 16:1153–1162

Ölveczky BP, Verkman AS (1998) Monte carlo analysis of obstructed diffusion in three dimensions: application to molecular diffusion in organelles. Biophys J 74:2722–2730

Reits EAJ, Neefjes JJ (2001) From fixed to FRAP: measuring protein mobility and activity in living cells. Nat Cell Biol 3:E145–E147

Sbalzarini IF, Hayer A, Helenius A, Koumoutsakos P (2006) Simulations of (an)isotropic diffusion on curved biological surfaces. Biophys J 90:878–885

Sbalzarini IF, Mezzacasa A, Helenius A, Koumoutsakos P (2005) Effects of organelle shape on fluorescence recovery after photobleaching. Biophys J 89:1482–1492

Seiffert S, Oppermann W (2005) Systematic evaluation of FRAP experiments performed in a confocal laser scanning microscope. J Microsc 220:20–30

Shvartsman DE, Donaldson JC, Diaz B, Gutman O, Martin GS, Henis YI (2007) Src kinase activity and SH2 domain regulate the dynamics of Src association with lipid and protein targets. J Cell Biol 178:675–686

Siggia ED, Lippincott-Schwartz J, Bekiranov S (2000) Diffusion in inhomogeneous media: theory and simulations applied to whole cell photobleach recovery. Biophys J 79:1761–1770

Sinnecker D, Schaefer M (2004) Real-time analysis of phospholipase C activity during different patterns of receptor-induced $Ca^{2+}$ responses in HEK293 cells. Cell Calcium 35:29–38

Sniekers YH, van Donkelaar CC (2005) Determining diffusion coefficients in inhomogenous tissues using fluorescence recovery after photobleaching. Biophys J 89:1302–1307

Sprague BL, McNally JC (2005) FRAP analysis of binding: proper and fitting. Trends Cell Biol 15:84–91

Sprague BL, Pego RL, Stavreva DA, McNally JC (2004) Analysis of binding reactions by fluorescence recovery after photobleaching. Biophys J 86:3473–3495

Tannert A, Voigt P, Burgold S, Tannert S, Schaefer M (2008) Signal amplification between G$\beta\gamma$ release and PI3K$\gamma$-mediated PI(3,4,5)P3 formation monitored by a fluorescent G$\beta\gamma$ biosensor protein and repetitive two component total internal reflection/fluorescence redistribution after photobleaching analysis. Biochemistry 47:11239–11250

Teruel MN, Meyer T (2000) Translocation and reversible localization of signaling proteins: a dynamic future for signal transduction. Cell 103:181–184

Tsay TT, Jacobson KA (1991) Spatial fourier analysis of video photobleaching measurements. Biophys J 60:360–368

Wedekind P, Kubitschek U, Heinrich O, Peters R (1996) Line-scanning microphotolysis for diffraction-limited measurements of lateral diffusion. Biophys J 71:1621–1632